25th ABCM International Congress of Mechanical Engineering
October 20-25, 2019, Uberlândia, MG, Brazil

COB-2019-0850
NUMERICAL SIMULATION OF NATURAL CONVECTION INSIDE A SQUARE ENCLOSURE WITH DIFFERENTIALLY HEATED SIDE WALLS USING OPENFOAM®

Luiz Paulo Borges Miranda
Daniel Dall'Onder dos Santos
Federal University of Uberlândia, Av. João Naves de Ávila 2121, Uberlândia, MG, 38408-100, Brazil
luiz.miranda@ufu.br
dallonder@ufu.br

Abstract. *Non-Newtonian fluids are present at several industrial processes, thus it is important to develop tools that consider this behavior when solving the balance equations. This paper seeks to verify an OpenFOAM® routine for permanent incompressible flows that adopt the generalized Newtonian fluid hypothesis to model the viscosity variation and the Boussinesq's approximation to model the buoyancy effects. The results obtained with the proposed routine were compared with the results found in the literature. Local parameters, as the vertical velocity and temperature profiles, and global parameters, as the mean Nusselt number, were analyzed. Bingham and power-law fluids were simulated. In some cases, an image analysis software was used to allow the numerical comparison of the analyzed parameters. The sum of squared errors (SSE), the coefficient of determination (r^2) and the root mean square error (RMSE) were used to evaluate the difference between the profiles shown in the literature and the profiles obtained with the proposed routine. All the obtained results showed good agreement with the literature results, even with the error introduced by the image analysis software.*

Keywords: *OpenFOAM®; natural convection; generalized Newtonian fluid; Boussinesq's Approximation*

1. INTRODUCTION

Several industrial processes involve flows where the apparent viscosity depends on the strain rate. Processed foods and chocolates; toiletries and cosmetics; drilling mud, lubricants and greases; construction materials; among others (Nirmalkar *et al.*, 2014) are some examples of these processes. Thus, it is important to develop tools to solve the balance equations of these flows considering this characteristic.

The heat transfer in non-Newtonian fluids can differ significantly from heat transfer in Newtonian fluids: the variation of the apparent viscosity changes how the fluid flows, therefore it also changes the way the fluid transfers heat. This is particularly true for viscoplastic fluids: the coexistence of the fluid-like (yielded) and solid-like (apparent unyielded) regions in the flow affect the characteristics of the flow and the heat transfers mechanisms, as in the apparent unyielded zones the convection heat transfer is restricted by the high viscosity and the low shear rate. To understand this phenomenon, several studies have been developed for different configurations: Turan *et al.* (2010) and Turan *et al.* (2011b) simulated two-dimensional steady-state natural convection in rectangular enclosures with differentially heated side walls for Bingham fluids and power-law fluids, respectively. Turan *et al.* (2011a) also studied the two-dimensional steady-state natural convection in rectangular enclosures with differentially heated side walls, but the influence of the aspect ratio of the enclosure was analyzed too. Baranwal and Chhabra (2017) studied the laminar natural convection heat transfer to Bingham plastic fluids from two cylinders confined in a square enclosure with a temperature gradient between the cylinders and the walls surfaces. Dutta *et al.* (2018) simulated a square cylinder confined in a square duct filled with a Bingham plastic fluid to investigate how the laminar natural convection is affected by tilt angle and fluid yield stress. The authors considered the condition of a temperature gradient between the cylinder surface and the duct walls.

This work aims to verify an OpenFOAM® routine to solve the balance equations of incompressible permanent flows, adopting the generalized Newtonian fluid hypothesis, which asserts that the apparent viscosity only depends on the local strain rate. The buoyancy effects are modeled by the Boussinesq's approximation (Boussinesq, 1903), which means that the density is considered constant, except on the term that computes the gravity acceleration, where the density is defined as a function of the temperature. The mechanical model is discretized by the finite volume method (Ferziger and Peric, 2002), and the system is solved by the SIMPLE algorithm (Patankar and Spalding, 1972).

OpenFOAM® is a open source software for computational fluid dynamics (CFD) written in the C++ object-oriented

language, distinguishing itself by its syntax for partial differential equations that closely resembles the equations being solved. These features facilitate the customization and extension of the existing codes, allowing users to develop routines that fit their needs. Favero *et al.* (2010) aimed to validate two solver routines developed by the authors, one written to solve internal flows of viscoelastic fluids and the other to solve free surface flows of viscoelastic fluids. Habla *et al.* (2011) also developed a new solver for the OpenFOAM® toolbox, which handles viscoelastic two-phase flows. Higuera *et al.* (2013) present a wave generation and active absorption boundary condition and validate it. These three works compare the results of their routines with relevant experimental, numerical and analytical results found in the literature.

Among the standard OpenFOAM® solvers (Greenshields, 2015), there is a solver for transient incompressible flows for non-Newtonian fluids. There are three main differences between this standard solver and the proposed routine: the mechanical model of the proposed routine adds the energy balance equation, the momentum balance equation has the Boussinesq's approximation term and the transient terms are not considered. To verify the proposed routine, the results obtained with it will be compared with the results shown by Turan *et al.* (2010) and Turan *et al.* (2011b). OpenFOAM® already has a function to model the power-law viscosity behavior, but a new function was compiled to represent equations of the bi-viscosity model (O'Donovan and Tanner, 1984), used to simulate the viscoplastic behavior as Turan *et al.* (2010) did.

2. METHODOLOGY

In this section, the mechanical model and the adopted hypothesis are presented. Then the geometry, the boundary conditions, and the mesh independence procedure are also shown. Finally, the adopted comparison criteria are defined.

2.1 Mechanical model

The fluid is assumed incompressible and the flow is at steady state. The continuity, momentum balance, and energy balance can be expressed as, respectively:

$$\begin{aligned} &\nabla \cdot \mathbf{u} = 0 \\ &\rho(\nabla \mathbf{u})\mathbf{u} = -\nabla p + \nabla \cdot \boldsymbol{\tau} + \rho \mathbf{g}\beta(T - T_c) \\ &\rho c_p(\nabla T)\mathbf{u} = \kappa \nabla^2 T \end{aligned} \tag{1}$$

where $\boldsymbol{u}$ is the velocity vector, ρ is the fluid density, p is the hydrostatic pressure, $\boldsymbol{g}$ is the gravity vector, β is the thermal expansion coefficient, T is the temperature, T_c is the reference temperature, in this case of the cold wall temperature, c_p is the fluid specific heat and κ is the thermal conductivity. c_p and κ are considered constants. $\boldsymbol{\tau}$ is the extra-stress tensor, and it is defined by the constitutive equation, as follows:

$$\boldsymbol{\tau} = 2\eta(\dot{\gamma})\mathbf{D}(\mathbf{u}) \tag{2}$$

where $\mathbf{D}(\mathbf{u})$ and the shear rate $\dot{\gamma}$ are defined as:

$$\mathbf{D}(\mathbf{u}) = \frac{1}{2}(\nabla \mathbf{u} + \nabla \mathbf{u}^T) \tag{3}$$

$$\dot{\gamma} = \sqrt{2tr\mathbf{D}(\mathbf{u})^2} \tag{4}$$

$\eta(\dot{\gamma})$ for the power-law case is defined as:

$$\eta(\dot{\gamma}) = K\dot{\gamma}^{n-1} \tag{5}$$

where K is the consistency index and n is the power-law index. For the Bingham fluid case, $\eta(\dot{\gamma})$ is modeled by the bi-viscosity constitutive equation:

$$\begin{aligned} &\eta(\dot{\gamma}) = \eta_0 && for\ \ \dot{\gamma} < \frac{\tau_0}{\eta_0} \\ &\eta(\dot{\gamma}) = \frac{\tau_0}{\dot{\gamma}} + \eta_\infty \left(1 - \frac{\tau_0}{\eta_0 \dot{\gamma}}\right) && for\ \ \dot{\gamma} \geq \frac{\tau_0}{\eta_0} \end{aligned} \tag{6}$$

where η_0 and η_∞ are, respectively, the viscosity for very low and high values of the shear rate and τ_0 is the yield stress limit of the material. To mimic the Bingham model, η_0 will be equal to $10000\eta_\infty$.

2.2 Dimensionless groups of interest

In this work, the dimensionless groups of interest are: the Rayleigh, Prandtl, and the Nusselt numbers. For the case of the Bingham fluid, a new dimensionless quantity is considered: the Bingham number.

The expressions for the Rayleigh (*Ra*) and Prandtl (*Pr*) numbers used in this work are:

$$Ra = \frac{\rho^2 c_p g \beta \Delta T L_c^3}{\eta_{nom} K} \tag{7}$$

$$Pr = \frac{\eta_{nom} c_p}{K} \tag{8}$$

where L_c is the characteristic length, taken as the value of the side of the square enclosure (*L*). η_{nom} is the nominal viscosity. For the power-law fluid case:

$$\eta_{nom} = K \left(\frac{\kappa}{\rho c_p L_c^2} \right)^{n-1} \tag{9}$$

and for the Bingham fluid case:

$$\eta_{nom} = \eta_\infty \tag{10}$$

The Nusselt number (*Nu*) and the convective heat transfer coefficient (*h*) are given by:

$$Nu = \frac{h L_c}{\kappa} \tag{11}$$

$$h = \frac{\kappa}{|T_{wall} - T_{ref}|} \left. \frac{\partial T}{\partial x} \right|_{wf} \tag{12}$$

where the subscript *wf* refers to the condition of the fluid in contact with the wall. T_{wall} is the temperature of the wall, and T_{ref} is the appropriate reference temperature, which can be taken to be the temperature of the cold wall when evaluating the Nusselt number over the hot wall, for example.

The Bingham *Bn* number is defined by:

$$Bn = \frac{\tau_0}{\eta_{nom}} \sqrt{\frac{L_c}{g \beta \Delta T}} \tag{13}$$

2.3 Geometry and boundary conditions

Figure 1 schematically shows the geometry domain analyzed by Turan *et al.* (2010). The vertical walls of the square enclosure are kept at different temperatures ($T_H > T_C$), and the horizontal walls are considered adiabatic. The no-slip condition is applied to each boundary. The temperatures of the cold wall and the hot wall are prescribed and constant. Turan *et al.* (2011b) adopt a similar geometry: the only difference is that the cold wall e hot wall positions are swapped. This difference does not compromise the comparison of the results obtained with the geometry shown in Fig. 1, as one geometry is the mirror image of the other.

The grid independence procedure was performed as described by Celik (2008), adopting the theoretical order of accuracy $p = 2$. This method is based on Richardson's extrapolation theory. The extrapolated value ϕ_{ext} is defined by $\phi_{ext} = (r_{21}^p * \phi 1 - \phi_2)/(r_{21}^p - 1)$, where ϕ is the analyzed parameter, r_{21} is the ratio between the representative length of the coarse mesh over the fine mesh. The subscripts indicate the mesh where that parameter was obtained: the subscript two represents the coarse mesh and subscript one refers to the fine mesh. The numerical uncertainties were estimated using the difference from extrapolation value and the obtained value in each mesh. For power-law fluids, three dimensionless sets were analyzed: n=1; n=0.6 and n=1.8, with $Ra = 10^6$ and $Pr = 100$. For Bingham fluids, two dimensionless sets were evaluated: Bn=0 and Bn=0.5, with $Ra = 10^4$ and $Pr = 7$. The chosen parameters to evaluate the grid were the maximum vertical velocity and the mean Nusselt number. The chosen mesh had a maximum of 4% error from the extrapolated value, providing a reasonable compromise between high accuracy and computational efficiency.

The adopted mesh has 100 elements in each direction and a total of 10000 elements. The mesh is finer at the boundaries, and coarser at the center of the geometry. Every element is rectangular and the minimum element length is equal to $3.6960 \times 10^{-3} \times L$, where *L* is the square enclosure length. For any direction (vertical or horizontal), when moving from

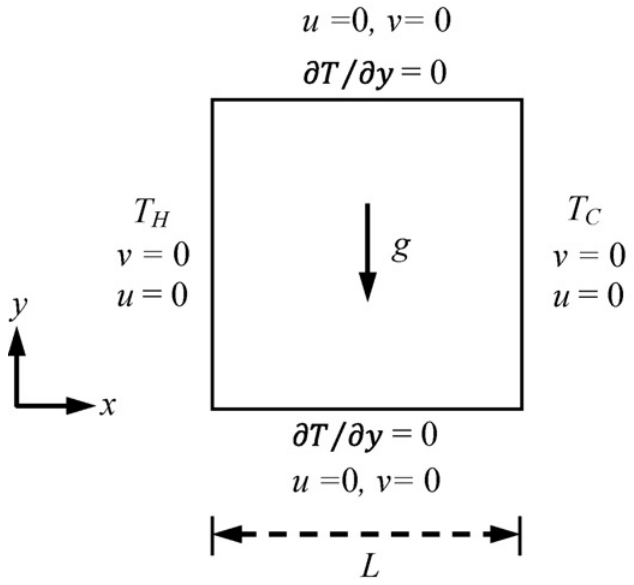

Figure 1. Schematic representation of the square enclosure. Image from Turan *et al.* (2010) .

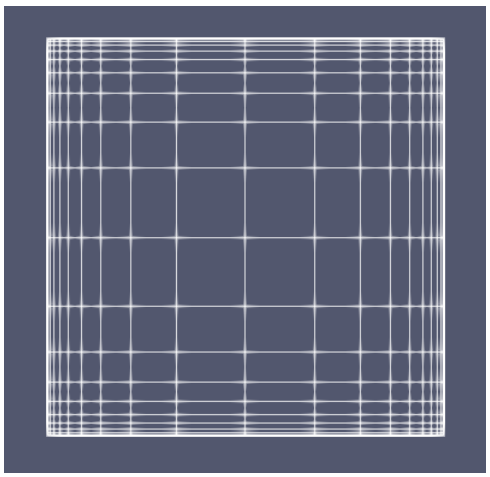

Figure 2. A 20x20 grid to illustrate how the mesh refinement near the boundaries is made.

the boundaries towards the center, the ratio between the length of two neighbor cells is equal to 1.0361. Figure 2 illustrate how the expansion rate works, with a mesh 20x20 and an expansion rate of 1.5137. Comparing the adopted mesh with the meshes adopted by Turan *et al.* (2010) and Turan *et al.* (2011b), all the three grids follows the same logic of refinement, but the mesh used by Turan *et al.* (2011b) has only 80x80 elements, whilst the grid used by the present work and by Turan *et al.* (2010) has 100x100 elements. The convergence criteria is set to 10^{-9} for every case.

2.4 Comparison criteria

As the main goal of this work is to verify a solver routine, it is important to establish the criteria to compare the obtained results with the results found in the literature. Several times, Turan *et al.* (2010) and Turan *et al.* (2011b) report the results in a graphic, as a temperature profile or a correlation of the studied parameters, for example. This imposes two main problems to compare the results: how to convert these curves to numerical values, and what criteria apply to evaluate the entire curve. To solve the first problem, an image analysis software was employed. This procedure can generate a significant error, especially when several curves overlap in a graphic, or when the scale of the graphic is not adequate. Once the graphics are converted to numerical data, three statistical criteria will were to evaluate the results obtained by the routine: the sum of squared errors (*SSE*), the coefficient of determination (r^2) and the root mean square error (*RMSE*). The *SSE* is a measure of the discrepancy between the data (in this case, the literature values) and an estimation model (the results obtained via the proposed routine). This way, the smaller the SSE, the better the routine is. r^2 provides a measure of how well the routine can replicate the data found in the literature, where a r^2 equals to one means the perfect fit of the data. *RMSE* is the square root of the average of squared errors, thus larger errors have an even larger effect, consequently, *RMSD* is sensitive to discrepant points, for example. Their numeric definition is:

$$SSE = \sum_{i=1}^{s} (\phi_i - \hat{\phi}_i)^2 \tag{14}$$

$$r^2 = 1 - \frac{SSE}{\sum_{i=1}^{s} (\phi_i - \bar{\phi})^2} \tag{15}$$

$$RMSE = \sqrt{\frac{SSE}{s}} \tag{16}$$

where *s* is the number of observations. ϕ_i is the reference value at the observation point i, $\hat{\phi}_i$ is the value obtained with the proposed routine at the observation point i and $\bar{\phi}$ is the mean value of the reference values.

When evaluating temperature or velocity profiles, all grid vertices over the specified axis will be evaluated as an observation point.

3. RESULTS

In this section, the obtained results are compared with the results found in the literature. The adopted properties for the comparison are the vertical velocity and temperature profiles, and the mean Nusselt number obtained with the power-law model.

3.1 Power-law fluid

This subsection will compare the results shown by Turan *et al.* (2011b) with the results of the proposed solver, using the power-law viscosity function that is part of the standard OpenFOAM® toolbox. For the temperature and vertical velocities profiles, 27 simulations were evaluated: all the combinations of three power-law index (*n*=0.6; *n*=1 and *n*=1.8), three Rayleigh number (*Ra*=10^4; *Ra*=10^5 and *Ra*=10^6) and three Prandtl number (*Pr*=10^2; *Pr*=10^3 and *Pr*=10^4). Figure 3 compares the vertical velocity and temperature profiles for some of the evaluated cases, as an example, and Tab. 1 shows the minimum r^2 and the maximum *RMSD* and *SSE* obtained with these 27 simulations.

Table 1. Minimum r^2 and the maximum *RMSD* and *SSE* for the vertical velocity and temperature profiles

	Vertical velocity	Temperature
r^2_{min}	0.9526	0.9603
$RMSD_{max}$	167.8212	0.0223
SSE_{max}	2.8445×10^6	0.0503

As can be seen in Fig. 3, several vertical velocity profiles overlap, and the magnitude of each profile is strongly affected by the power-law index. These two characteristics decrease the accuracy of the image analysis software. Even so, the r^2_{min} is still slightly below the unity, and most of the r^2 obtained are above 0.99. As the magnitude of the velocity profile is strongly affected by the power-law index, the interpretation of $RMSD_{max}$ and SSE_{max} is compromised, as a less relevant error in a high magnitude profile can generate a higher $RMSD_{max}$ and SSE_{max}, hiding more serious errors in others profiles. The temperature profiles have an even higher r^2_{min}. As the dimensionless temperature is always from 0 to 1, the image analysis software can capture the results with more accuracy, although the profiles continue to overlap. Also because of the same magnitude, the low $RMSD_{max}$ and SSE_{max} interpretation corroborate with the conclusion that the obtained results have a good agreement with Turan *et al.* (2011b).

Figure 4 shows a comparison of the mean Nusselt number results. Turan *et al.* (2011b) propose a correlation of the mean Nusselt number with *Pr*, *Ra*, and *n*. The values of the mean Nusselt number were compared with this correlation, and the results are exposed at Tab. 2. 108 simulations were used to achieve these results.

Table 2. r^2, *RMSD*, and *SSE* for the obtained mean Nusselt number, compared with the results of Turan *et al.* (2011b)

	Mean Nusselt number
r^2	0.9978
$RMSD$	0.3586
SSE	13.8877

The values of r^2, *RMSD*, and *SSE* confirm that the two methodologies have a good agreement. Some of the coefficients of correlation proposed by Turan *et al.* (2011b) were defined by a curve fitting process and the correlation is recommended for the following ranges: $10^4 \leq Ra \leq 10^6, 10 \leq Pr \leq 10^5$, and $0.6 \leq n \leq 1.8$. Thus it is expected to have a

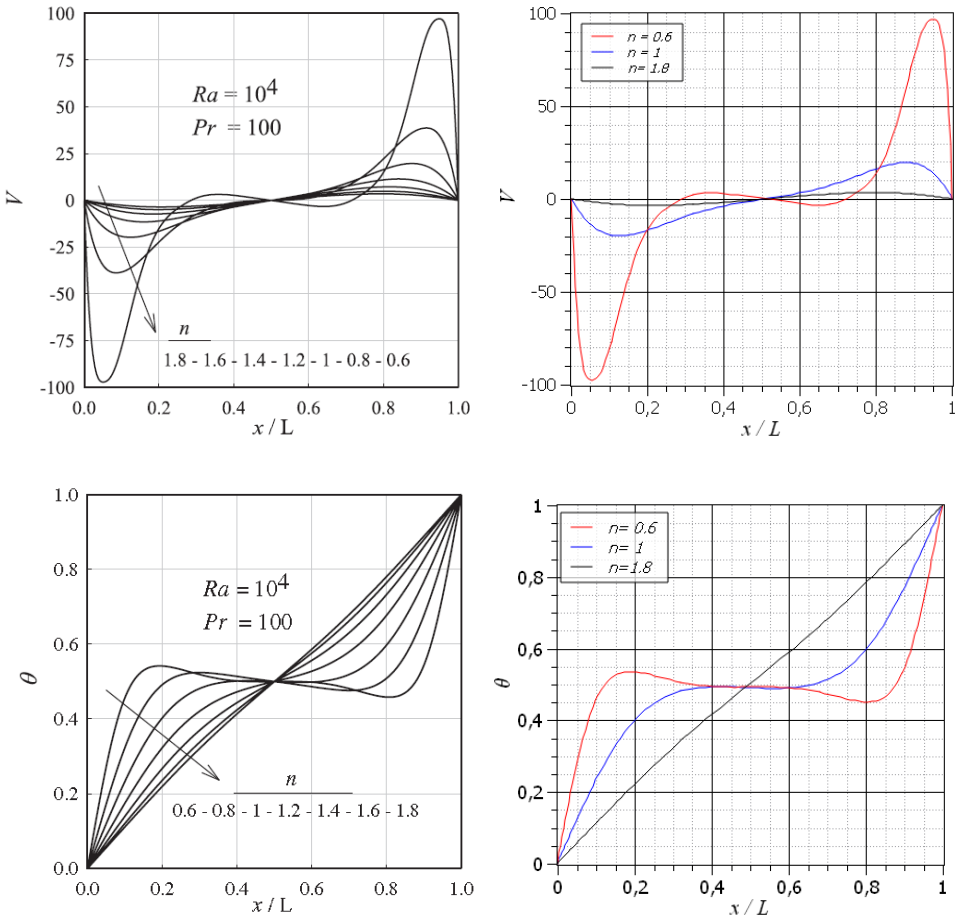

Figure 3. Temperature and vertical velocity profiles for Pr= 100, Ra=10^4, and a range of n. The graphs of the left column are from Turan *et al.* (2011b), and the graphs from the right column were obtained with the proposed routine

difference from the correlation and the simulated values, particularly when the parameters are near the correlation validity boundaries.

3.2 Bingham fluid

In this section, the fluid inside the square enclosure is modeled by the bi-viscosity model, with a high viscosity plateau for low shear rates, followed by a sudden drop of viscosity. To model this behavior, a new function was written by the authors. The results obtained with the proposed routine are compared with the results shown by Turan *et al.* (2010). The same methodology of the last subsection was employed, with the only difference that the correlation proposed by Turan *et al.* (2010) has three coefficients which values are obtained by a curve fitting method, and their values are not shown by the authors. Although a curve fitting method could be applied to estimate these coefficients, this methodology would induce a good agreement of the results, compromising the quality of the verification process. Thus, only results for the temperature and vertical velocity profiles were analyzed.

Once again, the image analysis software had problems to accurately convert the graphs into numerical data, particularly when several curves with different orders of magnitude are at the same graph. As can be seen in Fig. 5, this characteristic is critical for graphs of vertical velocity profiles with different Bn. Because of this, some results could not be compared, as the error introduced by the image analysis software renders the analysis impracticable. Figure 5 shows the temperature and vertical velocity profiles for Bn=0.5, Pr=7 and a range of Ra, Fig. 6 shows the temperature and vertical velocity profiles for Ra=10000, Pr=7, and a range of Bn,and Tab. 3 shows the minimum r^2 and the maximum *RMSD* and *SSE* for these simulations. Eight simulations were used to obtain these results.

All the parameters presented at Tab. 3 indicate a high correlation between the results of the proposed routine and the results shown by Turan *et al.* (2010). r^2 is particularly high for the temperature profile, this can be explained by the fact that the graph of temperature profiles for different Bn has less overlapping zones than the other graphs. This way, the image analysis software can capture with more accuracy each curve, and the error introduced by this methodology is minimized.

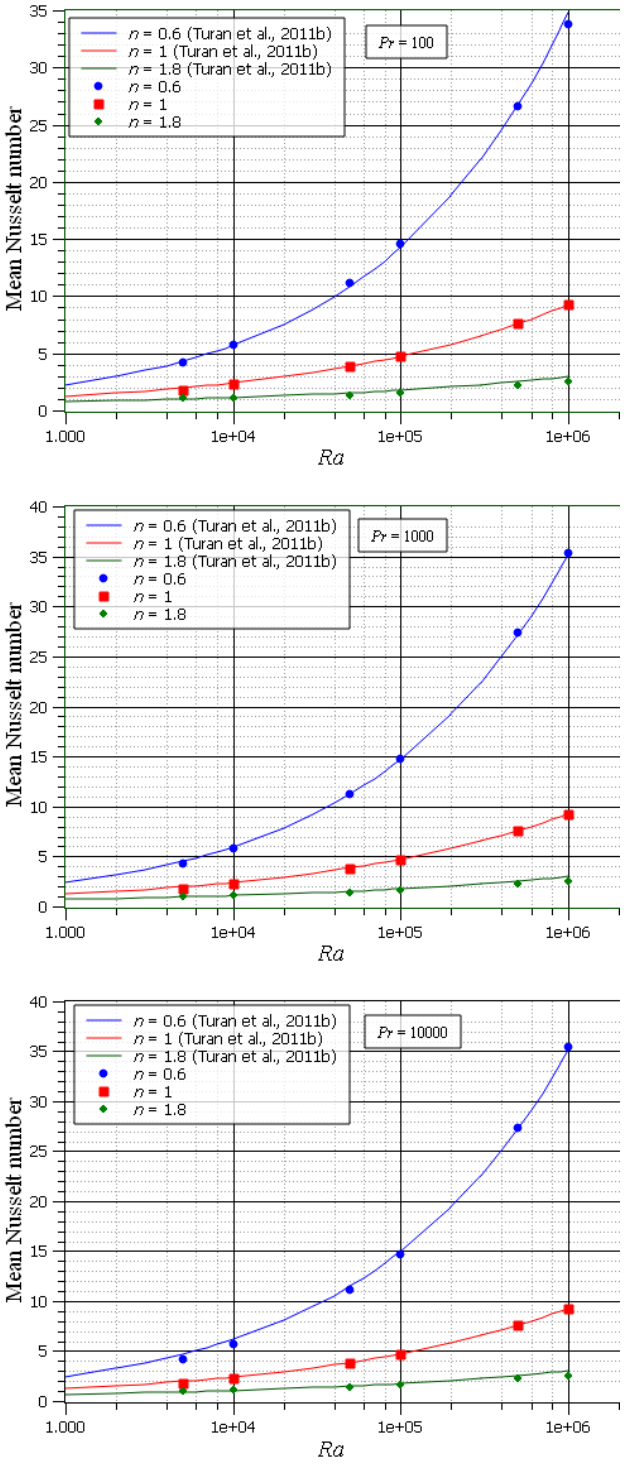

Figure 4. Nusselt as a function of *Ra*, for *Pr* = 100, *Pr* = 1000, and *Pr* = 10000. The continuous lines are the correlations proposed by Turan *et al.* (2011b), and individual values were obtained with the proposed routine.

Table 3. Minimum r^2 and the maximum *RMSD* and *SSE* for the vertical velocity and temperature profiles for Bingham fluids obtained comparing the results with Turan *et al.* (2010)

	Vertical velocity	Temperature
r^2_{min}	0.9605	0.9978
$RMSD_{max}$	5.3469	0.0077
SSE_{max}	2.8875×10^3	0.006

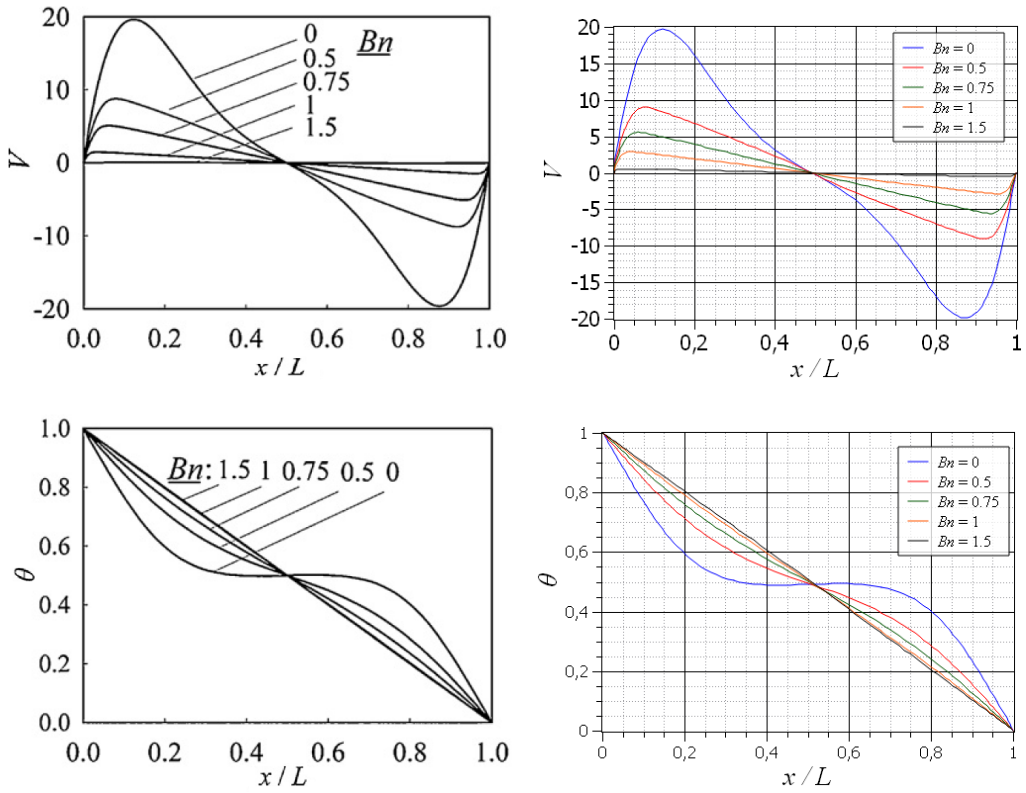

Figure 5. Vertical velocity and temperature profiles for Ra=10000, for Pr= 7, and a range of Bn : Bn= 0, Bn=0.5, Bn=0.75, Bn=1, and Bn=1.5. The graphs of the left column are from Turan *et al.* (2010), and the graphs from the right column were obtained with the proposed routine

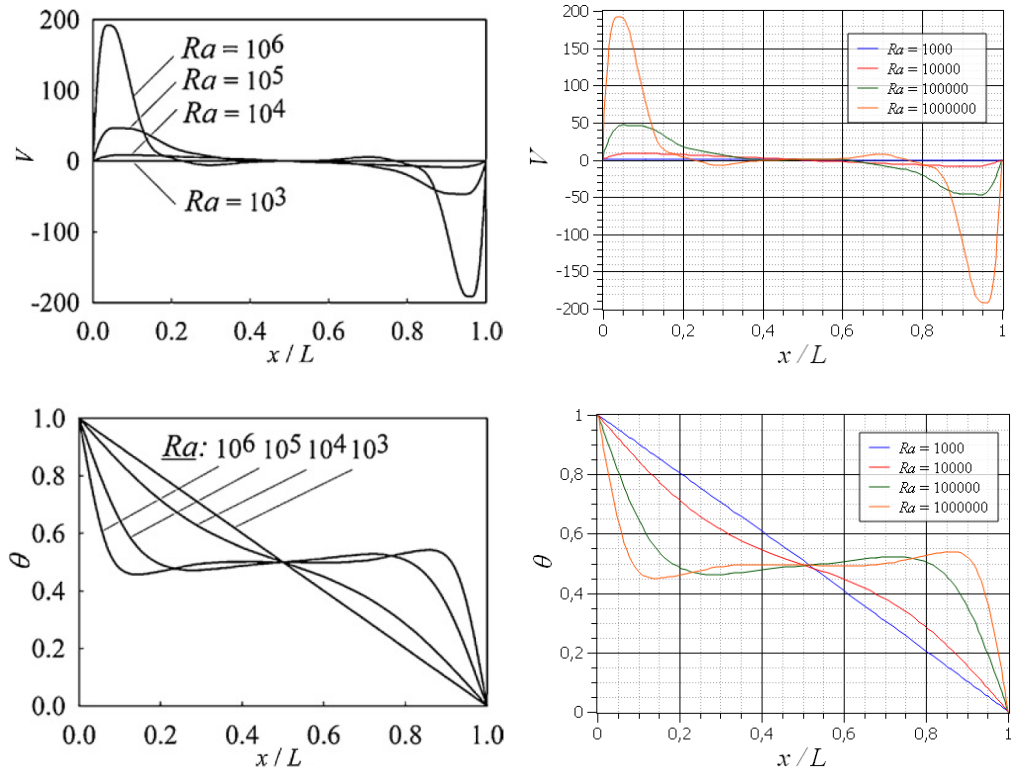

Figure 6. Vertical velocity and temperature profiles for Bn=0.5, for Pr= 7 and a range of Ra : Ra= 1000, Ra=10000, Ra=100000, and Ra=1000000. The graphs of the left column are from Turan *et al.* (2010), and the graphs from the right column were obtained with the proposed routine

4. CONCLUSION

In the present work, several simulations of natural convection inside a square enclosure with differentially heated side walls were made with an OpenFOAM® routine developed by the authors, and the results were compared with the results of Turan *et al.* (2010) and Turan *et al.* (2011b) to verify the routine. The main conclusions are:

- When comparing the vertical velocity and temperature profiles, for both power-law and Bingham fluids, the r^2 was always above 0.95, even with the error introduced by the image analysis software. These results lead to the conclusion that the OpenFOAM® routine can reproduce accurately the results of the literature.
- The mean Nusselt number results obtained with the power-law fluid were compared with the correlation proposed by Turan *et al.* (2011b). The obtained r^2, *RMSD*, and *SSE* indicate that the obtained results and the results found in the literature have a good agreement.
- The graphs that are more appropriated to the image analysis software have a significantly higher r^2, indicating that the image analysis software may be the main source of the error identified when comparing different curves.

5. ACKNOWLEDGMENTS

This study was financed in part by the Coordenação de Aperfeiçoamento de Pessoal de Nível Superior - Brasil (CAPES) - Finance Code 001.

6. REFERENCES

Baranwal, A.K. and Chhabra, R.P., 2017. "Effect of fluid yield stress on natural convection from horizontal cylinders in a square enclosure". *Heat Transfer Engineering*, Vol. 38, No. 6, pp. 557–577.

Boussinesq, J., 1903. *Thōrie analytique de la chaleur*, Vol. 2. Gauthier-Villars.

Celik, I.B., 2008. "Procedure for estimation and reporting of discretization error in cfd applications". *Journal of Fluids Engineering*, Vol. 130, No. 7, p. 078001.

Dutta, A., Gupta, A.K., Mishra, G. and Chhabra, R., 2018. "Effect of fluid yield stress and of angle of tilt on natural convection from a square bar in a square annulus". *Computers & Fluids*, Vol. 160, pp. 138–163.

Favero, J., Secchi, A.R., Cardozo, N. and Jasak, H., 2010. "Viscoelastic fluid analysis in internal and in free surface flows using the software openfoam". *Computers & chemical engineering*, Vol. 34, No. 12, pp. 1984–1993.

Ferziger, J.H. and Peric, M., 2002. *Computational methods for fluid dynamics*. Springer Science & Business Media.

Greenshields, C.J., 2015. "Openfoam programmer's guide". *OpenFOAM Foundation*.

Habla, F., Marschall, H., Hinrichsen, O., Dietsche, L., Jasak, H. and Favero, J.L., 2011. "Numerical simulation of viscoelastic two-phase flows using openfoam®". *Chemical engineering science*, Vol. 66, No. 22, pp. 5487–5496.

Higuera, P., Lara, J.L. and Losada, I.J., 2013. "Simulating coastal engineering processes with openfoam®". *Coastal Engineering*, Vol. 71, pp. 119–134.

Nirmalkar, N., Bose, A. and Chhabra, R.P., 2014. "Free convection from a heated circular cylinder in Bingham plastic fluids". *International Journal of Thermal Sciences*, Vol. 83, pp. 33–44.

O'Donovan, E. and Tanner, R., 1984. "Numerical study of the bingham squeeze film problem". *Journal of Non-Newtonian Fluid Mechanics*, Vol. 15, No. 1, pp. 75–83.

Patankar, S.V. and Spalding, D.B., 1972. "A calculation procedure for heat, mass and momentum transfer in three-dimensional parabolic flows". *International Journal Heat Mass Transfer*, Vol. 15, pp. 1787–1806.

Turan, O., Chakraborty, N. and R. J. Poole, N., 2010. "Laminar natural convection of Bingham fluids in a square enclosure with differentially heated side walls". *Journal of Non-Newtonian Fluid Mechanics*, Vol. 165, pp. 901–913.

Turan, O., Poole, R.J. and N. Chakraborty, N., 2011a. "Aspect ratio effects in laminar natural convection of Bingham fluids in rectangular enclosures with differentially heated side walls". *Journal of Non-Newtonian Fluid Mechanics*, Vol. 166, pp. 208–230.

Turan, O., Sachdeva, A., Chakraborty, N. and Poole, R.J., 2011b. "Laminar natural convection of power-law fluids in a square enclosure with differentially heated side walls subjected to constant temperatures". *Journal of Non-Newtonian Fluid Mechanics*, Vol. 166, No. 17-18, pp. 1049–1063.

7. RESPONSIBILITY NOTICE

The authors are the only responsible for the printed material included in this paper.